frontiers | Frontiers in Earth Science

DATA REPORT
published: 20 May 2022
doi: 10.3389/feart.2022.886975

Genesis of the Zhaoxian Gold Deposit, Jiaodong Peninsula, China: Insights From *in-situ* Pyrite Geochemistry and S-He-Ar Isotopes, and Zircon U-Pb Geochronology

Yiwen Xu[1], *Guangzhou Mao*[1,2]*, *Xiaotong Liu*[1,3], *Pengrui An*[1], *Yu Wang*[1] and *Mingping Cao*[1]*

[1]Shandong Provincial Key Laboratory of Depositional Mineralization and Sedimentary Minerals, College of Earth Sciences and Engineering, Shandong University of Science and Technology, Qingdao, China, [2]Functional Laboratory of Marine Mineral Resources Evaluation and Detection Technology, Qingdao National Laboratory of Marine Science and Technology, Qingdao, China, [3]Agency for Natural Resources of Rongcheng, Weihai, China

Keywords: pyrite chemistry, isotope geochemistry, Zhaoxian gold deposit, Jiaodong gold province, zircon U-Pb geochronology

OPEN ACCESS

Edited by:
Kit Lai,
Fortescue Metals Group, Australia

Reviewed by:
Guanglai Li,
East China University of Technology, China
Junming Yao,
Xinjiang Institute of Ecology and Geography (CAS), China

****Correspondence:***
Guangzhou Mao
gzmaonjunwu@163.com
Mingping Cao
cmp4688164@163.com

Specialty section:
This article was submitted to Economic Geology, a section of the journal Frontiers in Earth Science

Received: *01 March 2022*
Accepted: *11 April 2022*
Published: *20 May 2022*

Citation:
Xu Y, Mao G, Liu X, An P, Wang Y and Cao M (2022) Genesis of the Zhaoxian Gold Deposit, Jiaodong Peninsula, China: Insights From in-situ Pyrite Geochemistry and S-He-Ar Isotopes, and Zircon U-Pb Geochronology. Front. Earth Sci. 10:886975. doi: 10.3389/feart.2022.886975

INTRODUCTION

The Jiaodong gold province is located in the southeastern margin of the North China plate. The region is composed of a metamorphic basement (Jiaodong Group), multiple generations of magmatic rocks (Linglong and Guojialing plutons), and crosscut by many NE- and NNE-trending faults (**Figure 1B**) (Zhang et al., 2001; Goldfarb and Santosh, 2014; Li et al., 2015; Cheng et al., 2016; Chai et al., 2019). Jiaodong is the most important gold province in China, with three main types of gold mineralization, i.e., altered rock type (Jiaojia-type), quartz vein-type (Linglong-type) and brecciated- and massive type (Pengjiakuang-type), among which the former is more important (>80% of gold reserve in the gold province).

The Zhaoxian is a typical Jiaojia-type gold deposit, and is developed in the cataclastic/altered granite of the Jiaojia fault zone. Drilling shows mineralization at 1,500–2200 m depth, much deeper than most gold deposits (<800 m) in the region. Zhaoxian gold deposit is a typical representative of the Jiaojia type gold deposit. It is of great theoretical and practical significance to study the metallogenic characteristics of Zhaoxian gold deposit in detail, and provide theoretical support for further study of gold deposits in Jiaodong area.

Pyrite contains a wide range of trace elements, and their content/ratio and isotopes can reveal the metallogenesis and the nature/source and evolution of ore-forming fluids (Bi et al., 2004; Zhu et al., 2009; Mao et al., 2013; Reich et al., 2013; Tauson et al., 2013). Application of *in situ* analytical technology can avoid the mixing of different generations pyrite and improve the analysis resolution and speed (Huang et al., 2015; Zhang J. R. et al., 2016). In this study, therefore, we studied the pyrites from different hydrothermal mineralization stages, and analyzed their trace element and sulfur isotope compositions, as well as He-Ar isotopes of fluid inclusions in the pyrite. In addition, we conducted zircon U-Pb dating on the ore-related cataclastic granite to constrain the mineralization age.

GEOLOGICAL BACKGROUND

Regional Geology

The Jiaodong region is located east of the Tancheng-Lujiang fault, in the tectonic intersection between the North China Craton, Yangtze Craton, and the Qinling-Dabie Orogen (**Figure 1A**). The region is

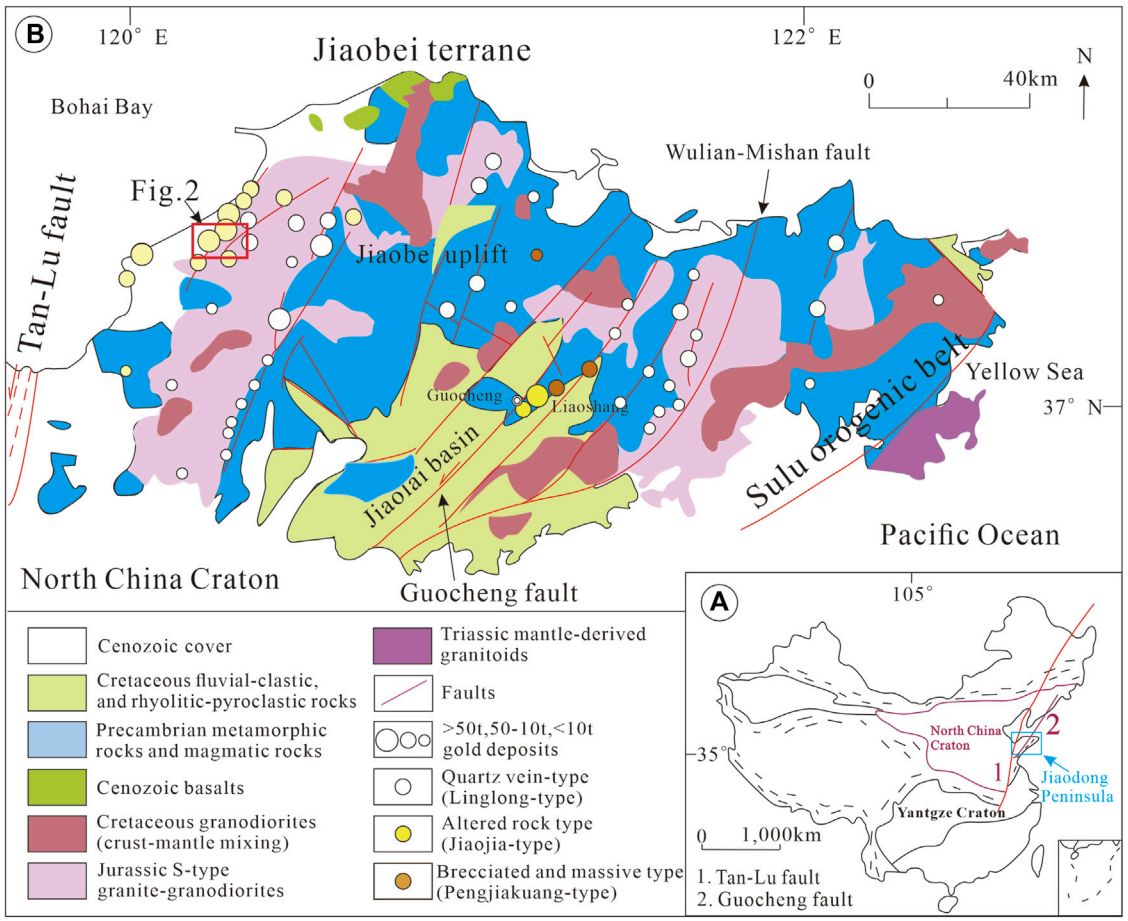

FIGURE 1 | Geologic map of the Jiaodong region **(A)**, showing the distribution of different types of gold deposits **(B)**. (after Deng et al., 2015).

composed of the Jiaobei Uplift in the north, the Jiaolai Basin in the middle, and the Sulu ultrahigh-pressure (UHP) metamorphic belt in the south (**Figure 1B**) (Li et al., 2007; Tan et al., 2012). From the Triassic to the Early Jurassic, the Precambrian North China and Sulu terranes were amalgamated along the NE-trending Wulian-Qingdao-Yantai fault, forming the basic tectonic framework of the Jiaodong gold province (Guo et al., 2017).

The region underwent greenschist-to granulite-facies metamorphism at ~1.9 Ga (Wang et al., 2017). The Sulu terrane is composed of a UHP metamorphic belt, and the basement rocks include mainly granitic gneisses and some mafic rocks (Zhao, 2016; Liu et al., 2018). The late Archean-Neoproterozoic strata are exposed in the region, and the Jurassic-Cretaceous strata are mainly exposed in the Jiaolai Basin (**Figure 1B**). Magmatic rocks are widespread and dominated by Yanshanian (Jurassic-Cretaceous) granites, which intruded the metamorphic basement. These granites are accompanied by Early Cretaceous dykes and volcanic rocks (Zhang, 2011; Zhao, 2016). NE-NNE faults are the main ore-controlling structures in the region, and include (from west to east) the Sanshandao, Jiaojia, Zhaoping, Xilin-Douya, and Jinniushan, in which 90% of the proven reserve in Jiaodong is distributed.

Deposit Geology

Zhaoxian gold deposit is located in the western margin of the Jiaobei Uplift and west of the Jiaojia fault (middle section), and the area is extensively covered by Quaternary sediments (**Figure 2**). Yanshanian intrusive rocks are well developed. Exploration drilling indicates that the Cuizhao Formation (of Linglong Group) is located in the northern and southern parts of the study area, whilst the Luanjiazhai Formation (of Malianzhuang Group) and Xinzhuang Formation (of Qixia Group) are located in the middle section. The deeper part of the mining area is bounded by the Jiaojia fault zone. The upper part of the stratigraphy comprises mainly the Luanjiazhai, Xinzhuang, and Cuizhao formations; whilst the lower part (ore-bearing) comprises the Cuizhao and Shangzhuang formations and locally the Guojialing pluton. Local basement structures include mainly nearly EW-trending ductile shear zones and NE-trending faults. The Jiaojia fault is the main ore-controlling structure, which is 160–500 m wide and W-/NW-dipping (strike: 0–30°). Dip angle of the northern and southern section is 10–26° (avg. 19°) and 12–40° (avg. 27°), respectively. The center of the

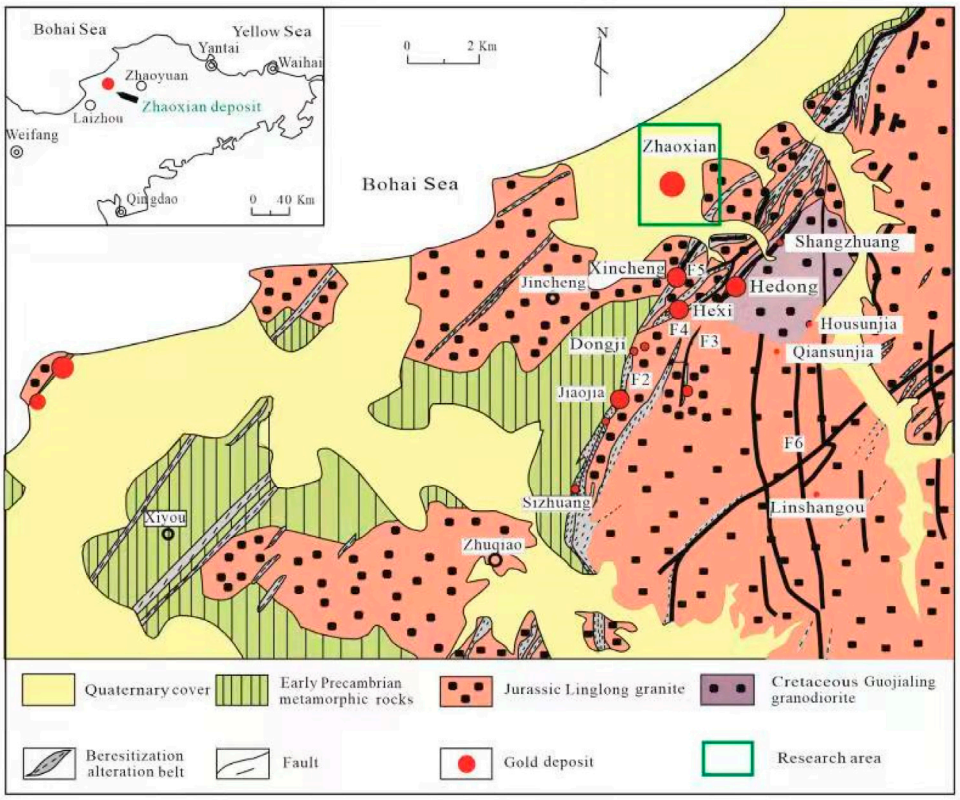

FIGURE 2 | Simplified geological map of the Zhaoxian gold deposit (modified from Li et al., 2015).

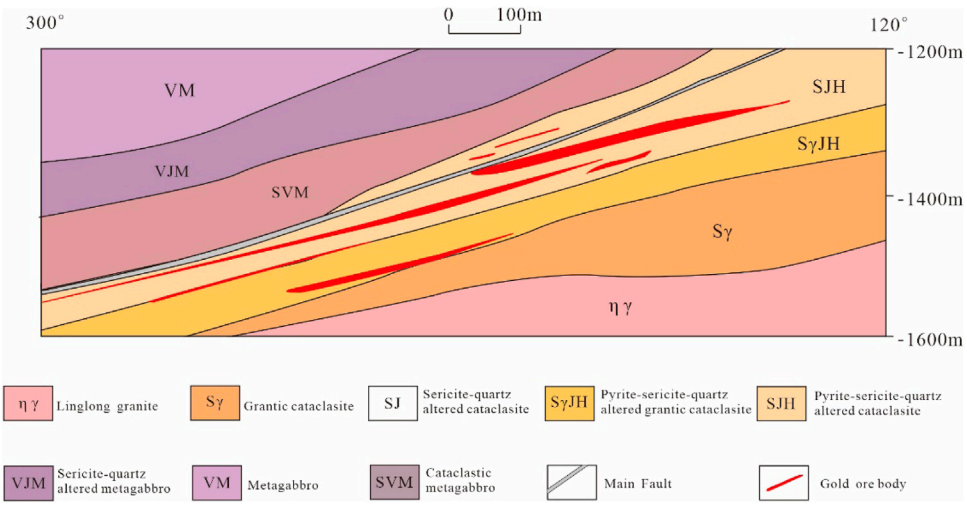

FIGURE 3 | Simplified cross-section of the Zhaoxian gold deposit.

main fault is marked by a dark-gray fault gouge (1–30 cm thick). From inside out, the fault comprises three zones with varying degrees of fragmentation: (1) mylonite and cataclastic zone (average thickness: ~20 m); (2) cataclastic granite and metagabbro (average thickness: ~50 m); (3) sericitized granite and metagabbro (average thickness: ~200 m). The boundaries between these three zones are mostly gradational. The vein/lenticular gold orebodies are mainly distributed in the pyrite-sericite-altered cataclastic rocks, close to the main fracture in the footwall (**Figure 3**).

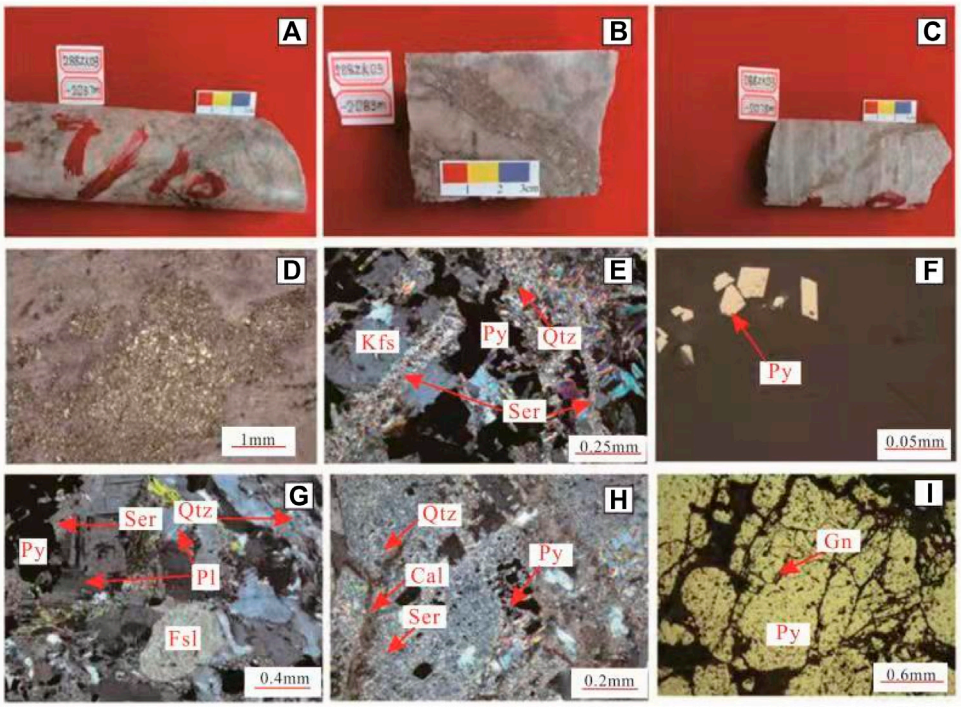

FIGURE 4 | Photos/photomicrographs of the pyrite-sericite-altered cataclastic granitic ore host: **(A–B)** hand-specimen of sericite-altered cataclastic granite and pyrite veins; **(C)** pyrite-sericite-altered cataclastic granite; **(D)** pyrite agglomerates; **(E)** pyrite with quartz, sericite, and altered K-feldspar residue; **(F–G)** granular pyrite with quartz (bent by stress) showing undulatory extinction; **(H)** pyrite metasomatized/corroded along margin, with clear embayment and skeletal structure; **(I)** pyrite broken with galena fracture infill. Kfs- K-feldspar; Qtz- Quartz; Ser- Sericite; Py- Pyrite; Pl- Plagioclase; Fsl-ferriferous augite; Cal- Calcite; Gn- Galena.

A total of 27 gold orebodies are delineated in Zhaoxian mining area, which can be divided into 4 orebody groups, from top to bottom were Ⅳ, Ⅰ, Ⅱ and Ⅲ. Ⅰ-1 and Ⅰ-2 orebodies are the main orebodies in Ⅰ orebody group. The length of Ⅰ-1 orebody is 1985 m, and the maximum dip length is 950 m. The ore body is large vein-like with the characteristics of expansion and contraction, SW- dipping at a dip angle varies from 11.20° to 19.00° and an average dip angle of 15.73°. The thickness of single project is 1.20–12.13 m, the average thickness is 3.55 m, and the variation coefficient is 92.92%. The single sample gold grade is (0.20–10.24) ppm, the average grade is 2.20 ppm, the variation coefficient is 72.79%, belongs to the orebody with uniform distribution of useful components.

Core logging reveals two main types of ore hosts: Pyrite-sericite-altered cataclastic granite (**Figures 4A,B**) and pyrite-sericite-altered cataclasite (**Figure 4C**). Ore structures include mainly disseminated, vein, and agglomerate (**Figures 4A–D**). Metallic minerals include mainly pyrite, followed by chalcopyrite, galena, sphalerite, and native gold (**Figures 4A–F**); whilst non-metallic minerals include quartz, K-feldspar, albite, sericite, chlorite, and calcite (**Figures 4E, G,H**). The ore textures include mainly granular, metasomatic, and cataclastic (**Figure 4I**).

According to the ore crosscutting relation and hydrothermal mineral assemblage, the mineralization of Zhaoxian gold deposit can be roughly divided into four stages. In chronological order, the four stages included (I) Pyrite-quartz-K-feldspar stage, (II) Pyrite-quartz-sericite stage, (III) Polymetallic sulfide-quartz stage and (IV) Quartz-calcite stage (**Table 1**). The first formed minerals often are metasomatism by the later formed minerals, or the late stage veins cut the early stage veins.

(I) Pyrite-quartz-K-feldspar stage: The pyrite grains are relatively coarse-grained (size: 1–6 mm), euhedral, and with relatively clean surface. The pyrite occurs as massive aggregates or veins, with occasional dissolution or fragmentation texture (**Figures 5A–C**). The quartz is coarse-grained, pure white, and deformed with local dynamic recrystallization and undulatory extinction (**Figure 5D**). K-feldspar grains are coarse, granular, and partially altered to sericite (**Figure 5D**). The content of gold in the ore is lower than that in Ⅱ and Ⅲ stages.

(II) Pyrite-quartz-sericite stage: Pyrite is fine-grained (mainly 50–300 μm) and euhedral with local dissolution features. The fine-grained quartz and sericite are altered from early plagioclase. At this stage, gold mainly exists as inclusions or in fissures (**Figures 5E–G**).

(III) Polymetallic sulfide-quartz stage: The fine-grained sulfides at this stage include galena, pyrite, chalcopyrite, and sphalerite (**Figure 5H**), and occur in quartz-sulfide veinlets or disseminations. Besides, fine-grained galena and chalcopyrite also occur as fracture infill in pyrite (**Figures 5I,J**). The quartz grains are fine and smoky-gray, whilst the gold occurs mainly as interstitial among or fracture-infill in galena, chalcopyrite, and pyrite (**Figures 5I,J**).

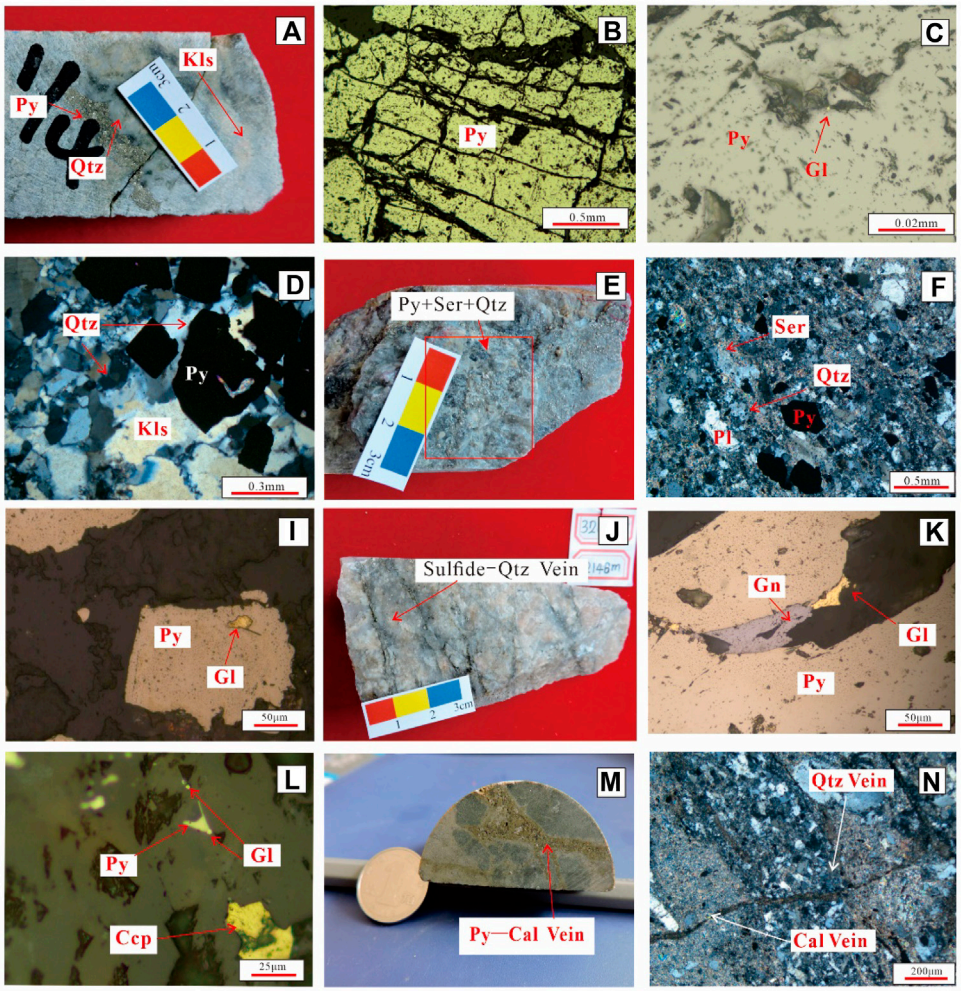

FIGURE 5 | Photos/photomicrographs of rocks and ores from the different mineralization stages of the Zhaoxian gold deposit [hand-specimen **(A,E,H,J,M)**; transmitted light **(D,F,L,N)** and reflected-light **(B,C,G,H,J,L)**]: **(A)** stage I pyrite aggregate; **(B)** stage I broken pyrite; **(C)** gold included in stage I pyrite; **(D)** quartz, K-feldspar (altered), and pyrite; **(E–F)** beresitization with fine mineral grains; **(I)** gold included in stage II pyrite; **(J)** quartz-polymetallic sulfide vein cut disseminated ore; **(K)** gold exists in fissure; **(L)** polymetallic sulfides coexist with gold inclusions; **(M)** coarse-grained stage IV pyrite-carbonate veins; **(N)** stage IV quartz and carbonate veins. Py- Pyrite; Qtz- Quartz; Kfs- K-feldspar; Gl-native gold; Ser- Sericite; Pl- Plagioclase; Gn- Galena; Ccp-Chalcopyrite; Cal- Calcite.

(IV) Quartz-calcite stage: Pyrite grains are coarse (size: up to 10 mm), cubic, and occur in veins/veinlets (**Figure 5K**) with quartz and calcite (**Figure 5L**).

Under the microscope, it is observed that stage II and III are the main gold ore stages, and gold mineralization is closely related to sericitization and silicification. The main gold-bearing minerals are pyrite, chalcopyrite, and galena. Native gold occurs commonly as interstitial or as inclusions or fracture-infill.

ANALYSES

The samples are all taken from drill cores (mainly 2038–2146 m depth). *In-situ* LA-ICP-MS pyrite trace element measurement was completed at the State Key Laboratory of Ore Deposit Geochemistry, Institute of Geochemistry, Chinese Academy of Sciences. The GeoLasPro laser ablation system was used, coupled with an Agilent 7700x ionization mass spectrometer. Analytical conditions include 10Hz pulse frequency, He carrier gas, and 23 μm (for fine-grained pyrite) or 33 μm (for coarse-grained pyrite) spot size. Elemental contents were calibrated against multiple reference materials (GSE-1G, BCR-2G, BIR-1G and BHVO-2G) and internal standardization (Dare et al., 2012). The recommended values of element concentrations for the USGS reference glasses are from the GeoReM database (http://crustal.usgs.gov/geochemical_reference_standards/microanalytical_RM.html). Detailed analytical procedures followed those described by Huang et al. (2016).

In-situ LA-ICPMS pyrite sulfur isotope analysis was completed at the State Key Laboratory of Geological Processes and Mineral Resources, China University of Geosciences (Wuhan). The Geolas2005 laser ablation system and Neptune

TABLE 1 | Mineralization stage and mineral paragenetic sequence.

Mineral	Ore stage			
	I	II	III	IV
K-feldspar				
Quartz				
Sericite				
Pyrite				
Chalcopyrite				
Sphalerite				
Galena				
Gold				
Calcite				

Plus Plasma mass spectrometer were used. Analytical conditions include 33 μm spot size, 10Hz pulse frequency, 50% T energy, 10.1–12.5V acceleration voltage, helium as a carrier gas, and argon as makeup gas. Detailed analytical procedures followed those described by Liu et al. (2008) and Fu et al. (2016).

The He-Ar isotope analysis of pyrite inclusions was completed at the Analytical and Testing Center in the Beijing Institute of Geological Research of Nuclear Industry. The Helix SFT™ Split Flight Tube noble gas mass spectrometer was used, with blank background less than 5×10^{-14} ccSTP, Faraday cup resolution higher than 400, and the ion multiplier resolution higher than 700. Sensitivity of the He and Ar measurements are better than 2×10^{-4} A/Torr and 1×10^{-3}A/Torr, respectively. Four samples (one in stage I, two in stage III, and one in stage IV) were measured. Stage II pyrite is not analyzed due to insufficient sample, and because stage II pyrite is mostly superimposed with pyrites of other stages (and thus prone to contamination). Detailed analytical procedures followed those described by Wang et al. (2016).

LA-ICP-MS zircon U-Pb dating was completed at the State Key Laboratory of Geological Processes and Mineral Resources, China University of Geosciences (Wuhan). Zircons used were all separated from the pyrite-sericite-altered cataclastic granite sample at the Hebei Langfang Keda Mineral Sorting Co. Ltd. The analysis used a GeoLas 2005 laser ablation system coupled with an Agilent 7500a plasma mass spectrometer. Analytical conditions include 24 μm spot size, 20–40 μm denudation depth, and 10Hz frequency. The U-Pb ages are corrected by using srm612 as external standard and 91500 and Plesovice as standard zircons. Detailed analytical procedures followed those described by Yuan et al. (2004).

RESULTS

Pyrite Trace Element Geochemistry

A total of pyrite 35 spots (stage I: 11, stage II: 9, stage III: 9, stage IV: 7) were analyzed, with the results shown in **Table 2**. The pyrite from the four stages has similar Fe (42.33–47.30 wt%) and S (52.19–57.33 wt%) contents, and the average pyrite S:Fe atomic ratios for stage I to IV are 2.08, 2.03, 2.10, and 2.16, respectively, higher than the theoretical value of 2:1, showing that the pyrite sample is Fe-poor, resembling pyrites from the Zhaoxian gold deposits (**Table 3**) and typical deep-level hydrothermal deposits (Cao et al., 2014). The pyrite Fe/(S + As) ratio can also indicate the mineralization depth, i.e., reaching 0.85 for deep-level mineralization and 0.86 for medium-level one, occasionally reaching 0.93 (Zhou et al., 2004; Barker et al., 2009; Cao et al., 2014). The Zhaoxian pyrite samples have Fe/(S + As) = 0.78 to 0.90, with the average value of different ore stages from 0.81 to 0.86. This indicates that the mineralization occurred in medium- to deep-level (more than 5000 m), consistent with the conclusion drawn from the S/Fe ratio.

Stage I pyrite has highest Co (avg. 697.91ppm) and Ni (avg. 46.51ppm) compared with the other three stages. Stage II pyrite has lower Co (avg. 152.391ppm) contents than stage I pyrite. Stage Ⅲ pyrite has lower Co (avg. 61.20 ppm) and Ni (avg. 25.91 ppm) contents than pyrite I and II. Stage Ⅳ pyrite has lowest Co (avg. 0.05 ppm) and Ni (avg. 13.31 ppm) compared with the other three stages.

Under high-temperature conditions, cobalt replaces Fe more readily in pyrite than Ni, leading to higher Co/Ni ratio. The average pyrite Co/Ni values decrease from stage I to IV (55.45, 46.73, 11.37, 1.1, respectively) (**Table 2**), suggesting a decrease of hydrothermal temperature from the early to late stage. Previous studies suggested that Co/Ni << 1 reflects sedimentary/diagenetic pyrite, whereas Co/Ni > 1 reflects magmatic hydrothermal pyrite. The Zhaoxian ore-related pyrite samples have overall Co/Ni ratio >1, suggesting a magmatic hydrothermal origin.

The stage I pyrite Co-Ni data points fall mostly in the hydrothermal field and minor in the magmatic field (**Figure 6**). This shows that early metallogenesis was closely hydrothermal-related with magmatic contribution. The stage II pyrite Co-Ni data points fall mainly (and almost equally) into the hydrothermal and magmatic fields. Compared with stage I

TABLE 2 | Pyrite trace element compositions of the Zhaoxian gold deposit.

No	Stage	S	Fe	Cu	Zn	Pb	Co	Ni	As	Te	Se	Mo	Au	Ag	Sn	Sb	W	Bi	Co/Ni	Au/Ag
A009	I	57.33	42.23	16.04	941.88	105.21	105	6.45	1153.34	1.86	2.33	0.04	0.46	5.62	0.22	1.81	0.01	5.91	16.31	0.08
A019	I	55.00	45.55	3.21	76.39	243.87	244	28.31	582.30	0.10	0.61	0.03	0.078	0.92	0.09	0.50	0.04	0.10	8.61	0.08
A021	I	54.58	47.25	60.12	106.86	410.52	411	4.34	234.68	—	1.04	0.06	0.022	1.47	0.21	1.13	0.07	2.91	94.59	0.02
A052	I	53.57	45.55	46.34	123.23	166.91	167	11.20	4474.43	0.24	—	0.02	1.20	8.92	0.17	1.85	0.004	9.55	14.91	0.13
B008	I	55.29	46.86	39.83	54.61	388.70	389	2.00	34.91	3.16	0.65	0.01	0.025	2.34	0.10	0.20	0.01	16.70	194.20	0.01
B009	I	52.03	44.71	1.25	317.75	304.58	305	3.18	55.50	1.35	0.50	—	0.019	6.95	0.03	—	0.005	17.38	95.88	0.003
A012	I	52.66	46.83	0.24	1.42	3371.26	3371	78.02	168.09	3.73	0.38	0.02	—	0.10	—	—	0.01	6.26	43.21	—
A015	I	50.40	46.65	11.63	131.79	1294.00	1,1294	241.62	297.38	4.75	—	0.07	0.16	3.90	0.11	0.35	0.28	17.65	5.36	0.04
A016	I	54.25	45.15	5.65	9.72	739.12	739	47.45	125.94	3.89	—	—	0.09	3.03	0.10	0.055	0.002	7.33	15.58	0.03
A017	I	55.87	46.33	2.23	8.03	379.23	379	3.21	15.79	1.65	0.56	0.004	0.08	2.35	—	0.032	0.01	2.62	118.15	0.03
A018	I	53.65	45.24	3.65	8.09	272.53	273	85.82	440.32	6.17	0.89	0.035	0.11	0.67	—	0.14	1.45	12.37	3.18	0.16
A019	II	54.05	47.30	28.24	442.59	76.52	76.5	4.11	3076.51	0.74	0.64	0.07	0.96	1.40	0.06	9.86	0.01	3.07	18.61	0.68
B007	II	52.59	46.43	0.93	1.62	619.26	619	236.86	19.39	1.11	1.11	0.01	0.024	0.02	0.08	0.044	0.07	2.13	2.61	1.35
B006	II	54.39	43.78	1.05	1.97	170.23	170	241.06	50.71	3.13	1.67	0.01	0.038	0.13	—	0.059	0.006	8.25	0.71	0.29
A021	II	52.92	46.23	17.15	260.66	232.33	232	140.90	793.12	19.83	0.18	—	1.13	27.8	0.02	0.88	0.002	28.19	1.65	0.04
B038	II	54.88	43.43	27.58	90.63	92.08	92.1	0.37	3532.83	—	—	0.013	0.92	10.9	—	3.42	0.006	4.43	249.43	0.08
B039	II	52.94	44.34	16.45	63.08	10.45	10.4	0.11	1967.86	0.19	0.89	0.005	0.85	7.07	—	4.96	0.01	3.79	92.01	0.12
B040	II	52.33	46.95	8.01	33.39	71.34	71.3	2.48	2277.44	0.18	1.39	—	0.51	2.71	0.09	1.93	0.01	8.19	28.76	0.19
A019	II	54.78	44.92	0.35	10.02	73.69	73.7	32.47	364.26	2.56	1.29	—	0.007	0.15	0.04	0.058	0.005	3.80	2.27	0.05
B037	II	52.19	44.91	14.08	42.46	26.45	26.5	1.08	2411.46	1.49	1.59	0.032	0.33	6.25	0.21	3.709	0.04	2.81	24.54	0.05
A053	III	54.70	43.58	26.58	25.61	106.38	106	3.26	18.02	2.77	0.66	—	0.16	4.85	0.04	0.012	0.003	14.10	32.67	0.03
B030	III	52.67	45.04	1.76	2.93	0.05	0.050	0.03	221.18	0.14	1.22	—	0.03	0.11	—	0.49	—	0.20	1.50	0.30
B031	III	53.45	45.25	0.34	2.22	4.77	4.77	0.09	973.71	0.22	—	0.01	0.001	0.004	0.15	0.006	0.005	0.01	53.49	0.20
A034	III	55.01	43.72	9.16	183.20	185.12	185	126.53	247.28	12.20	—	—	0.68	13.5	0.09	0.07	0.06	25.68	1.46	0.05
A035	III	53.69	45.35	1.44	20.62	112.60	113	39.71	205.13	4.96	0.16	0.02	0.10	0.60	0.20	0.08	0.05	21.55	2.84	0.17
A036	III	56.91	44.88	90.59	29.92	47.18	47.2	41.40	524.72	6.74	0.80	0.01	0.13	1.15	0.01	0.83	0.02	5.24	1.14	0.11
C040	III	55.64	46.24	4.42	12.65	4.84	4.84	2.74	23.05	0.83	0.71	0.005	0.036	0.77	0.05	0.11	—	4.52	1.77	0.05
A048	III	52.86	45.55	10.44	14.42	83.01	83.0	12.94	235.03	0.86	0.58	0.005	—	0.49	0.05	0.23	0.01	4.46	6.42	0.00
B018	III	55.01	47.25	0.19	2.92	6.97	6.97	6.47	516.03	0.31	—	—	0.008	0.02	—	—	—	0.04	1.08	0.38
A028	IV	54.55	45.55	59.46	42.90	0.17	0.17	249.37	1576.01	1.66	0.73	0.07	0.06	2.19	0.30	—	0.74	3.97	1.00	0.03
A031	IV	56.41	46.86	1.12	48.05	—	—	5.10	1.53	—	0.28	0.02	0.014	0.75	—	0.029	0.006	0.21	—	0.018
A032	IV	54.96	44.71	0.02	0.22	0.01	0.014	0.16	0.46	0.25	—	0.07	0.017	0.03	0.16	—	—	0.30	0.09	0.67
A034	IV	54.56	46.83	778.39	118.09	0.17	0.17	0.94	73.80	1.03	0.35	0.05	0.10	7.39	—	0.36	0.10	7.61	0.17	0.01
A091	IV	56.25	46.65	—	0.67	0.00	0.0035	28.07	1.02	—	0.04	0.06	0.027	0.04	—	0.011	0.004	0.63	—	0.72
A094	IV	54.63	45.15	—	0.70	0.02	0.018	33.46	0.07	—	0.64	0.07	0.011	0.06	0.21	0.078	0.01	0.57	—	0.19
A043	IV	54.67	46.33	0.93	5.35	0.06	0.056	3.94	3848.39	3.96	0.45	—	0.54	0.29	0.01	0.23	0.01	5.73	0.01	1.89

N.B. Except for Fe and S, concentrations of the other elements are expressed in ppm; "—": below the detection limit.

TABLE 3 | Atomic number ratio of S and Fe and Fe/(S + As) for the Zhaoxian ore-related pyrite.

Stage I			Stage II			Stage III			Stage IV		
Sample No	S/Fe	Fe/(S + As)	Sample No	S/Fe	Fe/(S + As)	Sample No	S/Fe	Fe/(S + As)	Sample No	S/Fe	Fe/(S + As)
A009	2.36	0.74	A019	2.08	0.84	A053	2.12	0.83	A028	2.13	0.82
A019	2.15	0.81	B007	1.95	0.90	B030	1.95	0.90	A031	2.26	0.77
A021	2.12	0.83	B006	2.09	0.84	B031	2.01	0.87	A032	2.14	0.82
A052	2.04	0.85	A021	1.98	0.88	A034	2.20	0.80	A034	2.11	0.83
B008	2.17	0.81	B038	2.15	0.81	A035	2.03	0.86	A091	2.25	0.78
B009	1.90	0.92	B039	1.98	0.88	A036	2.28	0.77	A094	2.11	0.83
A012	1.96	0.89	B040	1.96	0.89	C040	2.20	0.80	A043	2.13	0.81
A015	1.80	0.97	A019	2.12	0.82	A048	1.97	0.89	—	—	—
A016	2.08	0.84	B037	1.97	0.88	B018	2.14	0.82	—	—	—
A017	2.22	0.79	—	—	—	—	—	—	—	—	—
A018	2.03	0.86	—	—	—	—	—	—	—	—	—
Avg	2.08	0.85	Avg	2.03	0.86	Avg	2.10	0.83	均值	2.16	0.81

N.B. S/Fe (atomic ratio), Fe/(S + As) (concentration ratio).

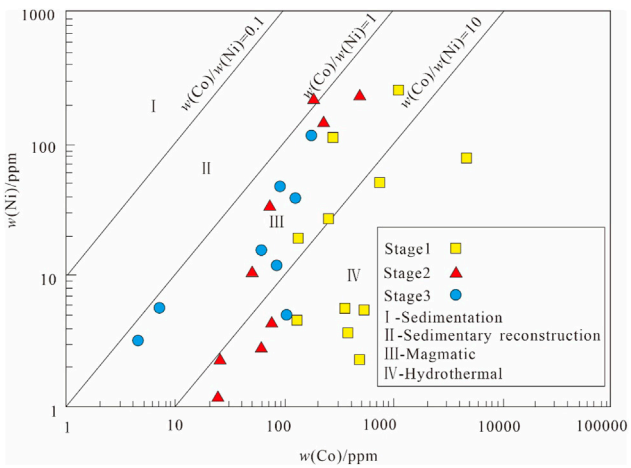

FIGURE 6 | Pyrite Ni-Co diagram for the Zhaoxian gold deposit (after Zhang C. et al., 2014).

pyrite, more pyrite data points of stage II fall into the magmatic field, suggesting more magmatic input. For stage III pyrite, the Co-Ni data points fall mainly into the magmatic field and minor into the hydrothermal field, indicating that the mineralization was closely magmatic-related. The stage IV pyrite Co-Ni data points fall outside the map, and it is a late stage of mineralization, the research significance is not important, so it will not be discussed.

Pyrite Sulfur Isotopes

A total of 31 pyrite sulfur isotope spot analyses were conducted, with the results shown in **Table 4**. The pyrite samples have $\delta^{34}S$ = 4.8–13.1%, with a range of 8.3%. Stage I pyrite (n = 10) has $\delta^{34}S$ = 9.6–13.1‰ (avg. 10.7‰); stage II pyrite (n = 10) has $\delta^{34}S$ = 7.2–10.1‰ (avg. 8.8‰); stage III pyrite (n = 7) has $\delta^{34}S$ = 4.8–6.7‰ (avg. 6.0‰); stage IV pyrite (*n* = 4) has $\delta^{34}S$ = 8.9–9.7‰ (avg. 9.2‰).

TABLE 4 | Pyrite $\delta^{34}S$ values of different hydrothermal stages in the Zhaoxian gold deposit.

No	Stage	$\delta^{34}S$ (‰)	Average $\delta^{34}S$ (‰)
1–2–1	I	13.1	10.7
1–2–3		12.9	
15–1		9.9	
15–2		9.7	
15–3		9.6	
15–4		9.8	
19–2		10.1	
19–4		10.7	
20–1		10.4	
20–2		10.4	
2–2–3	II	7.2	8.8
2–2–4		7.8	
2–2–5		8.8	
5–1		9.3	
5–2		10.1	
5–6		9.6	
9–2		7.6	
9–3		9.7	
11–4		8.8	
11–5		9.5	
1–1	III	6.7	6
1–2		4.8	
5–2		6.7	
9–4		6.6	
9–5		6.7	
12–2		5.0	
12–3		5.5	
3–1	IV	9.0	9.2
3–2		9.1	
3–3		9.7	
3–4		8.9	

The pyrite $\delta^{34}S$ values for the four stages are all positive and higher than the mantle-derived sulfur $\delta^{34}S$ range, suggesting possible multiple sulfur sources (Zhang W. Y. et al., 2014; Zhang R. Z. et al., 2016). **Figure 7** shows that the $\delta^{34}S$ range of the pyrite samples fall into the range of the altered rock-type

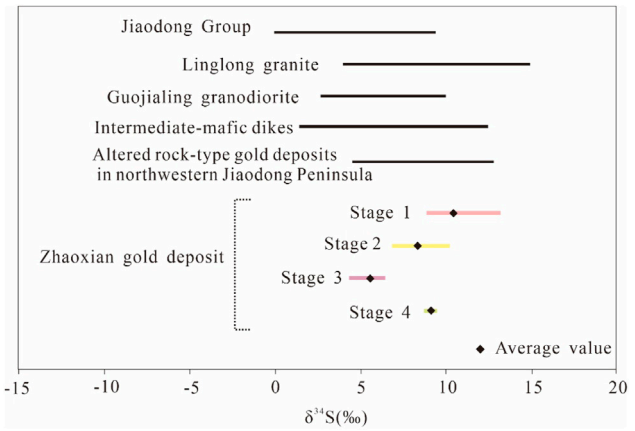

FIGURE 7 | $\delta^{34}S$ diagram of ore-related pyrite in the Zhaoxian gold deposit (modified after Zhang et al., 2014a and Wang, 2016).

gold ores from northwestern Jiaozhou. The higher $\delta^{34}S$ value for the stage I pyrite suggests that the sulfur source may have been the high $\delta^{34}S$ Linglong granite. The pyrite $\delta^{34}S$ value of stage II is slightly lower than that of stage I, suggesting both the Linglong granite and Guojialing granodiorite may have been a sulfur source. Stage III pyrite has the lowest $\delta^{34}S$ value (avg. 6.0‰), close to the average $\delta^{34}S$ value of the Guojialing granodiorite (6.7‰), and thus the latter may have been the sulfur source. During the gold mineralization (stage I to III), the average pyrite $\delta^{34}S$ value decrease from 10.7‰ (stage I) to 6.0‰ (stage III), similar to the trend shown in the neighboring Xincheng deposit (9.7‰ → 8.7‰ → 7.2‰) (Wang, 2016), suggesting similar source change/evolution. The metamorphic Jiaodong Group has $\delta^{34}S$ = 0–9.4‰ (mean 4.99‰) (Zhang C. et al., 2014; Wen et al., 2016), the Linglong granite has $\delta^{34}S$ = 4.0–15‰ (mean 9.5‰) (Li and Yang, 1993; Zhang W. Y. et al., 2014), and the Guojialing granite has $\delta^{34}S$ = 2.7–10.0‰ (mean 6.7‰). This implies that the Zhaoxian ore sulfur may have had similar source to other gold deposits in northwestern Jiaodong, possibly the Jiaodong Group and Mesozoic granites.

The $\delta^{34}S$ content of the Stage IV is higher than Stage II and Stage III, indicating that other fluids may have been mixed in the late stage of mineralization, and ore-forming materials are multi-source.

Fluid Inclusion He-Ar Isotopes

The ^{4}He content of the four samples is 5.199, 2.259, 2.029, and 3.709 × 10^{-8}ccSTP/g, respectively, whilst their $^{3}He/^{4}He$ = 55.4 ppb to 1.46 ppm (R/Ra = 0.04–1.04). The samples have ^{40}Ar = 4.954–11.899 × 10^{-8} and $^{40}Ar/^{36}Ar$ = 928.1–1,217.3 (**Table 5**). The R/Ra value of stage I and stage III is 15–21 times that of average crustal fluids, but lower than the minimum R/Ra of mantle fluids. This implies mantle fluid input during the mineralization. For stage IV samples, their R/Ra falls within the crustal fluid range, showing crustal inheritance. The mantle He content is also an index for evaluating the crust-mantle fluid mixing ratio (Yang et al., 2012; Wen et al., 2016). The proportion of mantle He in fluid inclusions from stage I and III pyrite is 10.02–13.11%, indicating that the coeval ore-forming fluids were mainly crustal-derived with minor mantle input. For stage IV, the proportion of mantle He is only 0.32%, indicating that the fluids were predominantly crustal-derived, consistent with the conclusion drawn from the R/Ra data (**Figure 8A**).

In the R/Ra-$^{40}Ar/^{36}Ar$ plot (**Figure 8B**), data points from stage I and III fall between the mantle and crustal end members, and stage I data points fall distal from the meteoric water field, suggesting legible meteoric water influence. In contrast, stage III data points fall close to the meteoric water field, implying probably meteoric water incursion during late mineralization. Stage IV data points falls inside the crustal fluid end member, consistent with the conclusion drawn from the ^{3}He-^{4}He plot.

Zircon U-Pb Age

Representative zircon CL images are shown in **Figure 9**. A total of 30 spots were analyzed, which yielded 20 concordant U-Pb ages. The results are listed in **Table 6**, and the zircon U-Pb age concordia diagram and weighted average age are shown in **Figure 10**.

For the concordant zircons, their U-Pb ages are 133–155 Ma (n = 16) and 190–252 Ma (n = 4). The zircons have 104–963 ppm U and 82–1,212 ppm Th, and their Th/U > 0.4.

DISCUSSION

Ore-Forming Material and Ore-Forming Fluids

Previous studies have suggested that the ore-forming material of gold deposits in northwestern Jiaodong Peninsula were mainly derived from the Jiaodong Group and/or mantle

TABLE 5 | Fluid inclusion He-Ar isotopic compositions of pyrite from the Zhaoxian gold deposit.

Sample	3	9	13	21
Mineral	Pyrite	Pyrite	Pyrite	Pyrite
Stage	IV	III	III	I
$^{3}He/10^{-14}$	0.017	2.375	3.300	5.723
$^{4}He/10^{-8}$	3.709	2.029	2.259	5.199
$^{3}He/^{4}He$ (R)	55.4 ppb	1.17 ppm	1.46 ppm	1.12 ppm
mantle He (%)	0.32	10.47	13.11	10.02
$^{40}Ar/10^{-8}$	4.954	7.104	7.911	11.899
$^{40}Ar/^{36}Ar$	934.6	940.2	928.1	1,217.3
R/Ra	0.04	0.84	1.04	0.80
$^{40}Ar^{*}/10^{-8}$	3.39	4.87	5.39	9.00
$^{40}Ar^{*}$ (%)	68.38	68.57	68.16	75.72
$^{40}Ar^{*}/^{4}He$	0.91	2.40	2.39	1.72
$F^{4}He$	65477.673	27892.847	27998.81	43689.071

Note: R: sample $^{3}He/^{4}He$ ratio; Ra: meteoric $^{3}He/^{4}He$ ratio, 1Ra = 1.4 ppm $^{40}Ar^{*}$ = radiogenic excess Ar after deducting air ^{40}Ar; $F^{4}He = (^{4}He/^{36}Ar)_{sample}/(^{4}He/^{36}Ar)_{air}$, $(^{4}He/^{36}Ar)_{air}$ = 0.1655; Isotopic content in cc·STP/g.

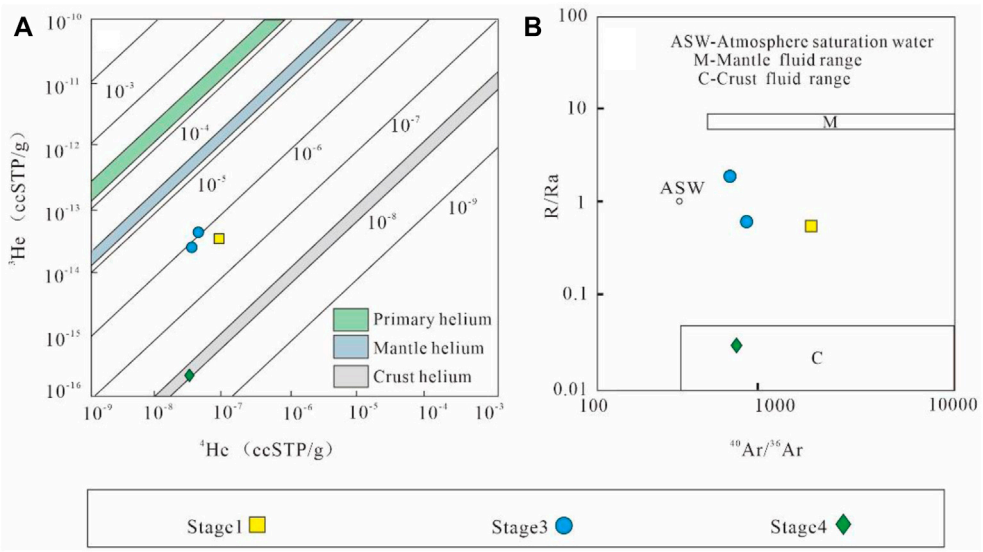

FIGURE 8 | Plots of ^{3}He-^{4}He **(A)**, R/Ra-$^{40}Ar/^{36}Ar$ **(B)** for the inclusions of ore-related pyrite from the Zhaoxian gold deposit (after Winckler et al., 2001; Zhang et al., 2012)

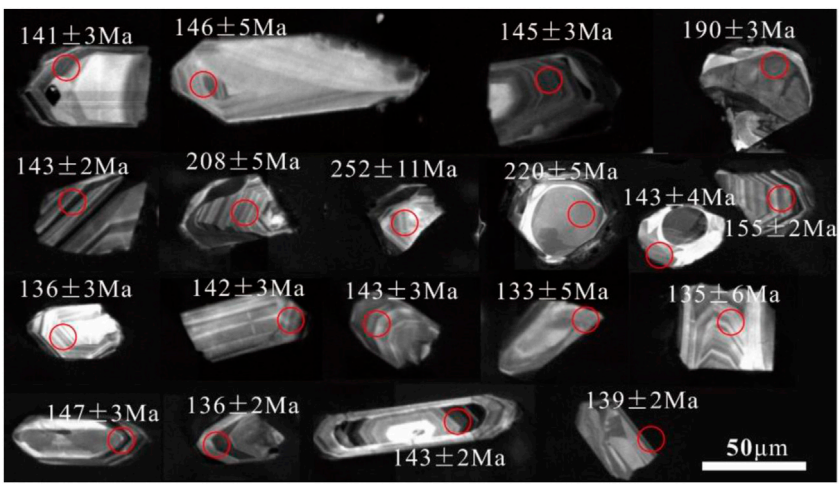

FIGURE 9 | Representative CL images for zircons from the Zhaoxian gold deposit.

(Deng et al., 2004; Li et al., 2007; Guo et al., 2008; Liang et al., 2015). However, the average Au content of the Jiaodong Group (2.47 ppb; Liu, 2016) is lower than the crustal average (4 ppb) (Li, 1976), while that of the Jiaodong Group in the Jiaojia Fault hangingwall at the Zhaoxian deposit is even lower (1.16 ppb). Therefore, it is assumed that the Jiaodong Group had supplied little material for the gold mineralization at Zhaoxian. In contrast, the average Au contents of the Linglong granite (19 ppb) and Guojialing granite (49 ppb) are high (Song et al., 2012), and represent a probably gold source. Previous studies have also suggested an upper-mantle gold source for the Jiaodong gold province (Gui, 2014). The magma may have extracted gold and other ore-forming elements from the upper mantle, and ascended to form the Linglong granite (Deng et al., 2004; Guo et al., 2005).

The pyrite $\delta^{34}S$ values are all positive and higher than the mantle-derived sulfur $\delta^{34}S$ range, suggesting possible multiple sulfur sources, possibly the Jiaodong Group and Mesozoic granites.

The pyrite trace element data show that the gold mineralization at Zhaoxian is closely related to magmatic-hydrothermal activity, with the ore fluids being magmatic-/metamorphic-sourced with brine input. Fluid inclusion He-Ar isotope compositions of pyrite suggest that the ore fluids

TABLE 6 | LA-ICP-MS zircon dating results for the Zhaoxian gold deposit.

Spot	Total Pb (ppm)	^{232}Th (ppm)	^{238}U (ppm)	Th/U	Isotopic ratio			Isotopic age		
					^{207}Pb/^{206}Pb	^{207}Pb/^{235}U	^{206}Pb/^{238}U	^{207}Pb/^{206}Pb	^{207}Pb/^{235}U	^{206}Pb/^{238}U
z1-1	17.895	332.54	383.24	0.94	0.0520 ± 0.0054	0.1569 ± 0.0165	0.0214 ± 0.0006	287 ± 23	148 ± 14	136 ± 4
z1-7	77.773	1,212.3	1780.8	0.82	0.0527 ± 0.0022	0.1651 ± 0.0067	0.0225 ± 0.0004	316 ± 96	155 ± 6	143 ± 2
z1-14	20.585	377.53	540.12	0.68	0.0457 ± 0.0031	0.1326 ± 0.0085	0.0214 ± 0.0004	153 ± 13	126 ± 7	136 ± 3
z1-39	22.433	251.11	615.25	0.70	0.0479 ± 0.0033	0.1418 ± 0.0085	0.0218 ± 0.0004	100 ± 155	134 ± 7	139 ± 2
z13-3	10.619	22.613	473.45	0.40	0.0533 ± 0.0036	0.2189 ± 0.0143	0.03 ± 0.0006	338 ± 14	200 ± 11	190 ± 3
z13-12	5.4935	2.9472	244.95	0.05	0.0516 ± 0.0034	0.2296 ± 0.0143	0.0329 ± 0.0008	264 ± 149	209 ± 11	208 ± 5
z13-17	5.0681	26.897	105.21	0.01	0.0519 ± 0.0075	0.2834 ± 0.0355	0.0399 ± 0.0019	283 ± 29	253 ± 28	252 ± 11
z13-20	5.2375	11.726	177.67	0.25	0.0556 ± 0.0042	0.2705 ± 0.0209	0.0348 ± 0.0008	438 ± 166	243 ± 16	220 ± 5
z13-6	31.681	277.76	184.2	1.54	0.0503 ± 0.0023	0.1582 ± 0.0078	0.0225 ± 0.0004	209 ± 10	149 ± 6.8	143 ± 2
z13-30	25.208	234.37	963.95	0.19	0.0485 ± 0.0024	0.1658 ± 0.0087	0.0244 ± 0.0005	120 ± 114	155 ± 7.5	155 ± 3
z13-32	15.164	318.8	291.56	0.24	0.0532 ± 0.0052	0.1627 ± 0.014	0.0226 ± 0.0007	338 ± 222	153 ± 12	144 ± 4
z20-1	76.266	314.33	335.46	1.00	0.0507 ± 0.0056	0.1463 ± 0.0142	0.0214 ± 0.0005	227 ± 237	138 ± 12	136 ± 3
z20-17	56.328	121.52	185.36	0.94	0.0510 ± 0.0044	0.1543 ± 0.0123	0.0223 ± 0.0005	242 ± 199	145 ± 10	142 ± 3
z20-20	24.165	258.26	620.31	0.65	0.0551 ± 0.0039	0.1664 ± 0.0109	0.0225 ± 0.0005	416 ± 159	156 ± 9	143 ± 3
z20-21	25.365	263.26	590.66	0.41	0.0551 ± 0.0085	0.1472 ± 0.0201	0.0209 ± 0.0008	416 ± 347	139 ± 17	133 ± 5
z20-23	32.265	296.56	685.26	0.44	0.0521 ± 0.0089	0.1506 ± 0.017	0.0212 ± 0.001	300 ± 342	142 ± 15	135 ± 6
z21-2	5.1737	125.62	123.83	0.43	0.0509 ± 0.0062	0.1491 ± 0.0162	0.0222 ± 0.0006	235 ± 259	141 ± 14	141 ± 3
z21-5	3.9352	82.003	104.27	1.01	0.0498 ± 0.0065	0.145 ± 0.0164	0.023 ± 0.0008	187 ± 277	137 ± 14	146 ± 5
z21-7	6.2455	126.56	182.76	0.78	0.0523 ± 0.0048	0.1588 ± 0.0132	0.0228 ± 0.0006	298 ± 209	149 ± 11	145 ± 3

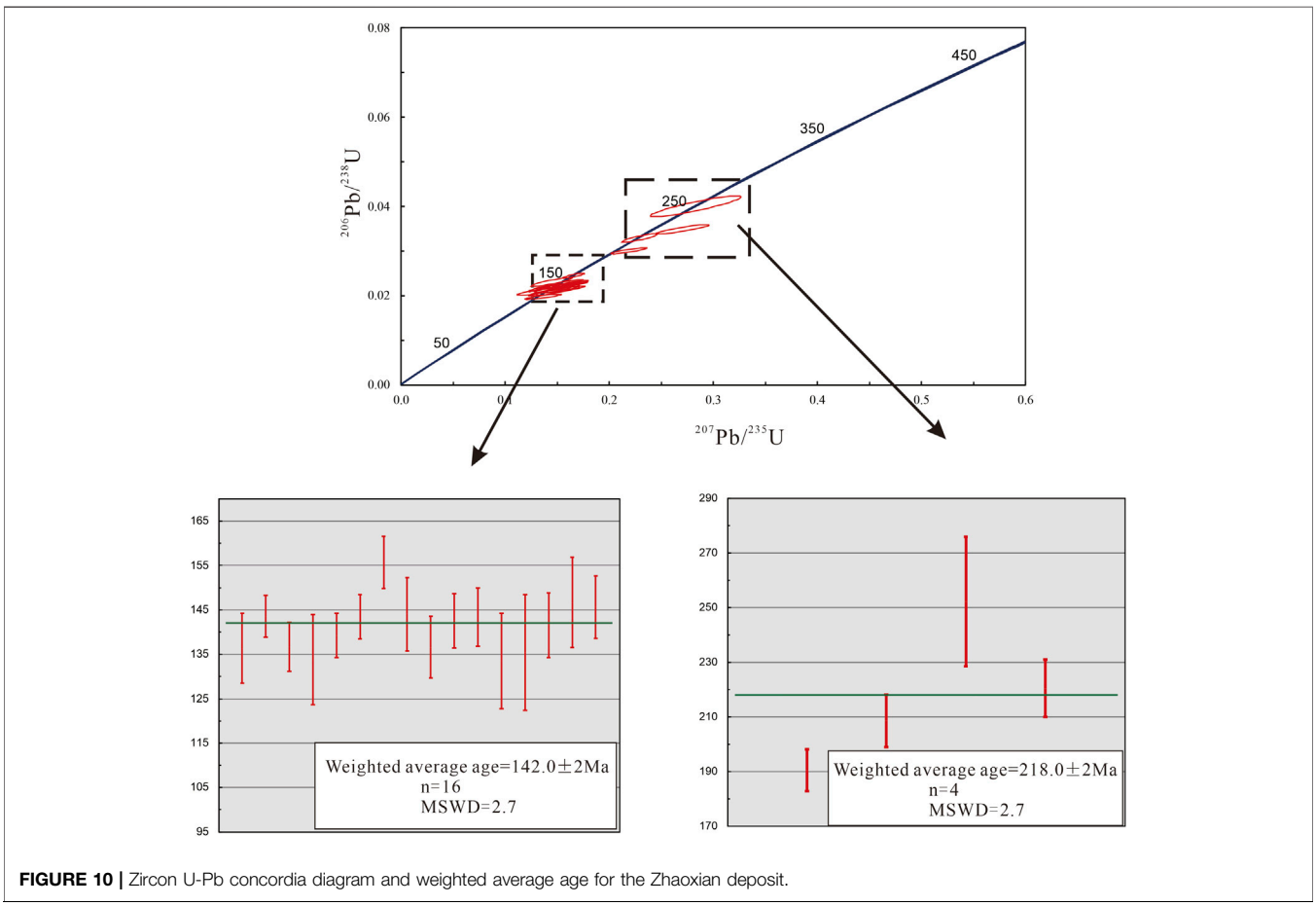

FIGURE 10 | Zircon U-Pb concordia diagram and weighted average age for the Zhaoxian deposit.

were characterized by crust-mantle mixing with minor meteoric water participation. Overall, the Zhaoxian ore-forming fluids were multi-sourced. The early-stage ore fluids were dominantly metamorphic-sourced, together with magmatic and (minor) brine input. Magmatic fluids played a more dominant role in the main-ore stage, in addition to brine and meteoric water contribution. Magmatic activity may have weakened toward the late-ore stage, and the ore fluids were mainly crustal-derived with negligible mantle input.

Therefore, we suggest that the ore-forming material and ore-forming fluids source may have been crust-mantle mixed, i.e., derived directly from the Linglong and Guojialing granites with inheritance from the Jingshan and Jiaodong groups.

Mineralization Age

Mesozoic magmatism in the Jiaodong region was extensive and multi-phase, and the timing was closely related to transformation of tectonic regimes (Deng et al., 2004; Wang et al., 2011). The major tectonic events in the northwestern Jiaojiang gold district were: (1) 240–216 Ma (or 245–220 Ma): the North China and Yangtze plates collided, forming the Dabie-Sulu collisional orogeny and initiating the Tanlu fault movement, accompanied by Indosinian magmatism (Deng et al., 2004; Chen et al., 2015); (2) ~140 Ma, the Paleo-Pacific subduction accelerated, causing large-scale sinistral shearing in the Tanlu fault zone and extensive mantle-derived magmatism (Deng et al., 2004); (3) 130–120 Ma: asthenospheric upwelling occurred due to regional extension, forming extensive magmatism. Pre-existing transpressive faults were transformed to transtensional shear, creating space for gold ore precipitation and concentration (Deng et al., 2004; Chen et al., 2015). At Zhaoxian, since the gold mineralization should occur after the granite ore-host emplacement (142 ± 2 Ma).

The zircon U-Pb ages of Zhaoxian gold deposit are divided into two groups. The first group average age is 243.0 ± 2 Ma, representing the Indosinian collision between the North China Plate and the Yangtze Plate. The other group average age is 142.0 ± 2 Ma, which represents the subduction event of the Pacific plate to the Eurasian plate and the formation time of the Linglong granites. Previous research results suggest that the gold deposit in Jiaodong area was formed in the transition period from extrusion to extension after the collision, later than the plate collision (Deng et al., 2004; Chen et al., 2015). We suggest that the gold mineralization is not earlier than 142 ± 2 Ma. The exact mineralization age would need more precise geochronological work to confirm.

Ore-Forming Processes

During the Late Jurassic (160–140 Ma), crustal delamination occurred in eastern North China, and extensive basement crustal remelting occurred in the northwestern Shandong. The magma may have extracted gold and other ore-forming elements from the upper mantle, and ascended to form the Linglong granite (Deng et al., 2004; Guo et al., 2005). The accelerated Paleo-Pacific subduction (~140 Ma) and collisional orogeny in Jiaodong may have formed a series of NNE-trending faults (e.g., the Zhaoping, Jiaojia, and Sanshandao-Cang Shang) in the Jiaobei Uplift and fractured the rocks along these fault zones, providing the fluid conduits and ore-deposition space. Meanwhile, the ascending magmas may have provided a heat source for the generation/circulation of metamorphic-/magmatic-sourced hydrothermal fluids, which formed the early-ore fluids. As the lithospheric thinning intensified, crust-mantle material mixing and partial melting occurred, and the ore-forming magma/fluids ascended along the deep fracture zones, forming the gold-rich Guojialing granodiorite (Deng et al., 2004; Chen et al., 2005). The subsequent fluid mixing (magmatic hydrothermal, brine, meteoric water) may have triggered ore deposition along structural traps.

CONCLUSION

(1) The Zhaoxian gold deposit comprises four hydrothermal stages, among which the second (pyrite-quartz-sericite-silicic) and third (polymetallic sulfide-quartz) stages are ore-forming. Pyrite is the main gold-bearing minerals, and native gold occurs as interstitial and in fissures and inclusions.

(2) The pyrite trace element and fluid He-Ar isotope characteristics show that the mineralization temperature decreased gradually, and the ore fluids were derived from a crustal-mantle mixed source, with metamorphic and magmatic fluids dominating the early and main ore stage, respectively, plus limited meteoric water input. The pyrite $\delta^{34}S$ values are positive across different hydrothermal stages, and the sulfur may have sourced mainly from the Linglong granite and Guojialing granite.

(3) Zircon U-Pb dating of the cataclastic granite ore host (142 ± 2 Ma) has constrained the maximum age for the Zhaoxian gold mineralization, coeval with the regional Yanshanian magmatism.

DATA AVAILABILITY STATEMENT

The original contributions presented in the study are included in the article/Supplementary Material, further inquiries can be directed to the corresponding authors.

AUTHOR CONTRIBUTIONS

GM is the corresponding author of this paper, responsible for comprehensive technical guidance in the research process, comprehensively analyzed the test data on the basis of comprehensive research, and comprehensively reviewed and finalized the article; YX is the first author of this paper. On the basis of field investigation and sample collection, she has carried out geochemical analysis and testing, and wrote the first draft of the paper; XL carried out the statistical analysis of sample microscopic observation and experimental data, and participated in the revision of the manuscript; PA participated in sample collection and data processing; YW participated in the field investigation and the

revision of the manuscript; MC contributed to the conception and design of the research. All authors contributed to manuscript revision, read, and approved the submitted version.

ACKNOWLEDGMENTS

We acknowledge Prof. Kit Lai and two reviewers for their valuable comments that improved the manuscript greatly. We thank the National Natural Science Foundation of China (42172087, 41572063) and the Key Laboratory of Gold Ore Formation Process and Resource Utilization (Ministry of Land and Resources) (2013003) for financial support of this work. The Guiyang Institute of Geochemistry (Chinese Academy of Sciences), the State Key Laboratory of Geological Processes and Mineral Resources [China University of Geosciences (Wuhan)], and the Beijing Institute of Geological Research of Nuclear Industry are thanked for supporting the laboratory analyses.

REFERENCES

Barker, S. L. L., Hickey, K. A., Cline, J. S., Dipple, G. M., Kilburn, M. R., Vaughan, J. R., et al. (2009). Uncloaking Invisible Gold: Use of Nanosims to Evaluate Gold, Trace Elements, and Sulfur Isotopes in Pyrite from Carlin-type Gold Deposits. *Econ. Geology.* 104 (7), 897–904. doi:10.2113/gsecongeo.104.7.897

Bi, X. W., Hu, R. Z., and Peng, J. T. (2004). REE and HFSE Geochemical Characteristics of Pyrites in Yao'an Gold deposit: Tracing Ore Forming Fluid Signatures. *Bull. Mineralogy, Petrol. Geochem.* 23 (1), 1–4. doi:10.3969/j.issn.1007-2802.2004.01.001

Cao, S. Q., Jia, J. S., and Zhong, Z. Q. (2014). Composition and Sulfur Isotope Characteristics of Auriferous Pyrite from the Shilongtou Gold deposit in Kaihua, Western Zhejiang Province. *Acta Petrologica Et Mineralogica* 33 (5), 937–946.

Chai, P., Zhang, H. R., Dong, L., and Zhang, Z. Y. (2019). Geology and Ore-Forming Fluids of the Dayingezhuang Gold deposit, Jiaodong Peninsula, Eastern China: Implications for mineral Exploration. *J. Geochemical Exploration* 204, 224–239. doi:10.1016/i.gexplo.2019.06.001

Chen, J., Sun, F. Y., and Wang, L. (2015). Zircon U-Pb Geochronology and Petrogeochemistry of Luanjiahe Granite in Jiaodong Region and Their Geological Significance. *Glob. Geology.* 34 (2), 283–295. doi:10.3969/j.issn.1004-5589.2015.02.003

Chen, Y.-J., Pirajno, F., and Qi, J.-P. (2005). Origin of Gold Metallogeny and Sources of Ore-Forming Fluids, Jiaodong Province, Eastern China. *Int. Geology. Rev.* 47 (5), 530–549. doi:10.2747/0020-6814.47.5.530

Cheng, S. B., Liu, Z. J., Wang, Q. F., Wang, F. J., Xue, Y. S., Xu, L., et al. (2016). Mineralization Age and Geodynamic Background for the Shangjiazhuang Mo deposit in the Jiaodong Gold Province, China. *Ore Geology. Rev.* 80, 876–890. doi:10.1016/j.oregeorev.2016.08.018

Dare, S. A. S., Barnes, S.-J., and Beaudoin, G. (2012). Variation in Trace Element Content of Magnetite Crystallized from a Fractionating Sulfide Liquid, Sudbury, Canada: Implications for Provenance Discrimination. *Geochimica et Cosmochimica Acta* 88, 27–50. doi:10.1016/j.gca.2012.04.032

Deng, J., Liu, X., Wang, Q., and Pan, R. (2015). Origin of the Jiaodong-type Xinli Gold deposit, Jiaodong Peninsula, China: Constraints from Fluid Inclusion and C-D-O-S-Sr Isotope Compositions. *Ore Geology. Rev.* 65, 674–686. doi:10.1016/j.oregeorev.2014.04.018

Deng, J., Wang, Q. F., and Yang, L. Q. (2004). The Geological Settings to the Gold Metallogeny in Northwestern Jiaodong Peninsula, Shandong Province. *Earth Sci. Front.* 11 (4), 527–533.

Fu, J. L., Hu, Z. C., Zhang, W., Yang, L., Liu, Y. S., Li, M., et al. (2016). *In Situ* Sulfur Isotopes ($\delta^{34}S$ and $\delta^{33}S$) Analyses in Sulfides and Elemental Sulfur Using High Sensitivity Cones in Combination with the Addition of Nitrogen by Laser Ablation MC-ICP-MS. *Analyt. Chim. Acta* 911 (16), 14–26. doi:10.1016/j.aca.2016.01.026

Goldfarb, R. J., and Santosh, M. (2014). The Dilemma of the Jiaodong Gold Deposits: Are They Unique? *Geosci. Front.* 5 (2), 139–153. doi:10.1016/j.gsf.2013.11.001

Gui, F. (2014). *Mineralization Enrichment Regularity and the Genesis Discussed of Sanshandao Gold deposit Shandong Province Laizhou*. China: Jilin University.

Guo, B., Liu, Z. C., and Li, W. (2008). Geological Features of Sanshan Island Gold Ore Formation and Future of Ore Search. *Mining Eng.* 6 (4), 14–16.

Guo, J. H., Chen, F. K., and Zhang, X. M. (2005). Evolution of Syn-To post-collisional Magmatism from north Sulu UHP belt, Eastern China: Zircon U-Pb Geochronology. *Acta Petrologica Sinica* 21 (4), 1281–1301.

Guo, L.-N., Goldfarb, R. J., Wang, Z.-L., Li, R.-H., Chen, B.-H., and Li, J.-L. (2017). A Comparison of Jiaojia- and Linglong-type Gold deposit Ore-Forming Fluids: Do They Differ? *Ore Geology. Rev.* 88, 511–533. doi:10.1016/j.oregeorev.2016.12.003

Huang, X.-W., Gao, J.-F., Qi, L., Meng, Y.-M., Wang, Y.-C., and Dai, Z.-H. (2016). *In-situ* LA-ICP-MS Trace Elements Analysis of Magnetite: The Fenghuangshan Cu-Fe-Au deposit, Tongling, Eastern China. *Ore Geology. Rev.* 72, 746–759. doi:10.1016/j.oregeorev.2015.09.012

Huang, X.-W., Gao, J.-F., Qi, L., and Zhou, M.-F. (2015). *In-situ* LA-ICP-MS Trace Elemental Analyses of Magnetite and Re-os Dating of Pyrite: The Tianhu Hydrothermally Remobilized Sedimentary Fe deposit, NW China. *Ore Geology. Rev.* 65, 900–916. doi:10.1016/j.oregeorev.2014.07.020

Li, S,X., Liu, C. C., and An, Y. H. (2007). *Geology of Gold Ores in Jiaodong*. Beijing: Geological Publishing House, 27–188.

Li, T. (1976). Earth Abundance of Chemical Elements. *Geochemistry* (3), 167–174.

Li, Y.-J., Li, S.-R., Santosh, M., Liu, S.-A., Zhang, L., Li, W.-T., et al. (2015). Zircon Geochronology, Geochemistry and Stable Isotopes of the Wang'ershan Gold deposit, Jiaodong Peninsula, China. *J. Asian Earth Sci.* 113, 695–710. doi:10.1016/j.jseaes.2015.03.036

Li, Z. L., and Yang, M. Z. (1993). *Geochemistry of Gold Deposits in Jiaodong*. Tianjin: Tianjin Science and Technology Press, 1–300.

Liang, Y. Y., Liu, X. F., and Liu, L. L. (2015). The Micro-geochemical Characteristics of Gold from "Altered Fracture-type" Gold deposit in Jiaodong Peninsula. *Acta Petrologica Sinica* 31 (11), 3441.

Liu, F. X. (2016). *Mineralization Enrichment Regularity and the Genesis Discussion of Xincheng Gold deposit*. China: Laizhou Shandong , Jilin University.

Liu, L. S., Liu, F. L., and Ji, L. (2018). The Polygenetic Meta-Granitic Rocks and Their Geological Significance, within the North Sulu Ultrahigh-Pressure belt. *Acta Petrologica Sinica* 34 (6), 1557–1580.

Liu, Y., Hu, Z., and Gao, S. (2008). *In Situ* Major and Trace Elements of Anhydrous Analysis Minerals LA-ICP-MS without Applying an Internal Standard. *Chem. Geology.* 257 (1-2), 34–43. doi:10.1016/j.chemgeo.2008.08.004

Mao, G., Hua, R., Long, G., and Lu, H. (2013). Rb-Sr Dating of Pyrite and Quartz Fluid Inclusions and Origin of Ore-Forming Materials of the Jinshan Gold Deposit, Northeast Jiangxi Province, South China. *Acta Geologica Sinica - English Edition* 87 (6), 1658–1667. doi:10.1111/1755-6724.12166

Reich, M., Deditius, A., Chryssoulis, S., Li, J.-W., Ma, C.-Q., Parada, M. A., et al. (2013). Pyrite as a Record of Hydrothermal Fluid Evolution in a Porphyry Copper System: A SIMS/EMPA Trace Element Study. *Geochimica et Cosmochimica Acta* 104 (1), 42–62. doi:10.1016/j.gca.2012.11.006

Song, M., Yi, P., Xu, J., Cui, S., Shen, K., Jiang, H., et al. (2012). A Step Metallogenetic Model for Gold Deposits in the Northwestern Shandong Peninsula, China. *Sci. China Earth Sci.* 55, 940–948. doi:10.1007/s11430-012-4366-7

Tan, J., Wei, J., Audétat, A., and Pettke, T. (2012). Source of Metals in the Guocheng Gold deposit, Jiaodong Peninsula, North China Craton: Link to Early Cretaceous Mafic Magmatism Originating from Paleoproterozoic Metasomatized Lithospheric Mantle. *Ore Geology. Rev.* 48 (5), 70–87. doi:10.1016/j.oregeorev.2012.02.008

Tauson, V. L., Babkin, D. N., and Akimov, V. V. (2013). Trace Elements as Indicators of the Physicochemical Conditions of mineral Formation in Hydrothermal Sulfide Systems. *Russ. Geology. Geophys.* (54), 526–543. doi:10.1016/j.rgg.2013.04.005

Wang, F., Lin, J. R., and Hu, Z. H. (2017). Isotopic Characteristics of Metallogenic Fluid and its Genesis in Yunji Uranium deposit of Xiangshan. *World Nucl. Geosci.* 34 (1), 9–13.

Wang, G. Q. (2016). *Mineralization of the Xincheng Gold Deposit, Northwest Jiaodong Peninsula: Multiple Isotope Tracer*. Beijing): China University of Geosciences.

Wang, Q., Deng, J., Liu, X., Zhao, R., and Cai, S. (2016). Provenance of Late Carboniferous bauxite Deposits in the North China Craton: New Constraints on Marginal Arc Construction and Accretion Processes. *Gondwana Res.* 38, 86–98. doi:10.1016/j.gr.2015.10.015

Wang, S. J., Wang, Y. S., and Guo, R. P. (2011). SHRIMP Zircon Dating of Linglong Type (Superunit) Granite in Eastern Shandong Province. *Shandong Land Resour.* 27 (4), 1–7. doi:10.3969/j.issn.1672-6979.2011.04.001

Wen, B.-J., Fan, H.-R., Hu, F.-F., Liu, X., Yang, K.-F., Sun, Z.-F., et al. (2016). Fluid Evolution and Ore Genesis of the Giant Sanshandao Gold deposit, Jiaodong Gold Province, China: Constrains from Geology, Fluid Inclusions and H-O-S-He-Ar Isotopic Compositions. *J. Geochemical Exploration* 171, 96–112. doi:10.1016/j.gexplo.2016.01.007

Winckler, G., Aeschbach-Hertig, W., and Kipfer, R. (2001). Constraints on Origin and Evolution of Red Sea Brines from Helium and Argon Isotopes. *Earth Planet. Sci. Lett.* 184 (3-4), 671–683. doi:10.1016/s0012-821x(00)00345-9

Yang, M., Wang, J. L., and Wang, J. Q. (2012). Helium and Argon Isotopic Tracing of Ore-Forming Fluid from the Wangfeng Gold Deposit in Xinjiang. *Acta Geoscientica Sinica* (5), 794–800. doi:10.3975/cagsb.2012.05.10

Yuan, H., Gao, S., and Liu, X. (2004). Accurate U-Pb Age and Trace Element Determinations of Zircon by Laser Ablation Inductively Coupled Plasma-Mass Spectrometry. *Geostandards Geoanalytical Res.* 28 (3), 357–370. doi:10.1111/j.1751-908x.2004.tb00755.x

Zhang, C., Liu, Y., and Liu, X. D. (2014a). Characteristics of Sulfur Isotope Geochemistry of the Xincheng Gold deposit, Northwest Jiaodong, China. *Acta Petrologica Sinica* 30 (9), 2495–2506.

Zhang, J. (2011). *A Geochemistry Study of Mesozoic Magmatism Rocks in the Sulu Orogeny*. HeFei: University of Science and Technology of China.

Zhang, J. R., Hou, L., and Zhou, Z. C. (2016a). LA-ICP-MS *In Situ* Trace Element Analysis of Auriferous Arsenic Pyrites from the Nibao Gold deposit and its Constraints on the Ore Genesis. *Acta Petrologica et Mineralogica* 35 (3), 493–505. doi:10.1007/s11434-009-0047-0

Zhang, L. C., Zeng, Q. D., and Zhou, W. L. (2001). Deep-seated Geochemistry and Prediction for the Denggezhuang Gold deposit in Jiu Dong. *Geology. Exploration* 37 (1), 27–29. doi:10.3969/j.issn.0495-5331.2001.01.006

Zhang, R. Z., Wang, Z. L., and Wang, S. R. (2016b). Metallogenic Mechanism of Dayingezhuang Gold deposit, Northwestern Jiaodong Peninsula: Geochemistry Constrains from the Gold Bearing Pyrite Typomorph and Sulfur Isotope. *Acta Petrologica Sinica* 32 (8), 2451.

Zhang, W. Y., Wang, C. Z., and Wei, X. C. (2014b). The Implications and Typomorphic Characteristics of Pyrite Chemical Composition in Zijinshan Gold-Copper Deposit. *Adv. Earth Sci.* 29 (8), 974–984. doi:10.11867/j.issn.1001-8166.2014.08.0974

Zhang, X., Li, S. R., and Lu, J. (2012). H-O, He-Ar Isotope Compositions of the Fluid Inclusions for Tracing the Source of Ore-Forming Fluids Jinchiling Gold deposit in Zhaoyuan, Shandong Province. *Bull. Mineralogy, Petrol. Geochem.* 32 (1), 40–47.

Zhao, R. (2016). *Tectonic Evolution and Gold Mineralization in the Jiaodong Peninsula*. Beijing): China University of Geosciences.

Zhou, X. W., Li, S. R., and Lu, L. (2004). Research on the Composition Typomorphism of Pyrite from Longkeng Gold-Silver Mineralization District in Wuyi, Zhejiang Province, China. *Bull. Mineralogy, Petrol. Geochem.* 24 (4), 6–13. doi:10.3969/j.issn.1007-2802.2005.04.006

Zhu, L. M., Zhang, G. W., and Guo, B. (2009). He-Ar Isotopic System of Fluid Inclusions in Pyrite from the Molybdenum Deposits in South Margin of North China Block and its Trace to Metallogenetic and Geodynamic Background. *Chin. Sci Bull* 54, 1725–1735. doi:10.1007/s11434-009-0047-0

Conflict of Interest: The authors declare that the research was conducted in the absence of any commercial or financial relationships that could be construed as a potential conflict of interest.

Publisher's Note: All claims expressed in this article are solely those of the authors and do not necessarily represent those of their affiliated organizations, or those of the publisher, the editors and the reviewers. Any product that may be evaluated in this article, or claim that may be made by its manufacturer, is not guaranteed or endorsed by the publisher.